Brain (2001), **124,** 2014–2027

In vivo visualization of activated glia by [^{11}C] (*R*)-PK11195-PET following herpes encephalitis reveals projected neuronal damage beyond the primary focal lesion

Annachiara Cagnin,[1] Ralph Myers,[1] Roger N. Gunn,[1] Andrew D. Lawrence,[4] Tom Stevens,[3] Georg W. Kreutzberg,[5] Terry Jones[1] and Richard B. Banati[1,2]

[1]*MRC Cyclotron Unit, Imperial College, Faculty of Medicine, Hammersmith Hospital,* [2]*Department of Neuropathology and Psychiatry, Imperial College, Faculty of Medicine, Charing Cross Hospital,* [3]*St Thomas' Hospital, London,* [4]*MRC Cognition and Brain Sciences Unit, Cambridge, UK and* [5]*Department of Neuromorphology, Max Planck Institute for Neurobiology, Martinsried, Germany*

Correspondence to: Richard B. Banati, MD, MRC Cyclotron Unit, Imperial College, Faculty of Medicine, Hammersmith Hospital, Du Cane Road, London W12 ONN, UK
E-mail: richard.banati@csc.mrc.ac.uk

Summary

A major challenge in the assessment of brain injury and its relationship to the ensuing functional deficits is the accurate delineation of the areas of damage. Here, we test the hypothesis that the anatomical distribution pattern of activated microglia, a normally dormant population of resident brain macrophages, can be used as a surrogate marker of neuronal injury not only at the primary lesion site but also in the antero- and retrograde projection areas of the lesioned neurones. Two patients with asymmetrical herpes simplex encephalitis were serially scanned 6 and 12 months after the acute illness using PET with [^{11}C] (*R*)-PK11195, a marker of activated microglia/brain macrophages. The evolving structural changes in the brain were measured by volumetric MRI and compared with the pattern of [^{11}C](*R*)-PK11195 binding. Corresponding to the clinically observed cognitive deficits, quantitative [^{11}C](*R*)-PK11195-PET revealed highly significant signal increases within the affected limbic system and additionally in areas connected to the limbic system by neural pathways, including the lingual gyrus in the occipital lobe and the inferior parietal lobe, which had normal morphology on structural MRI. The increased [^{11}C](*R*)-PK11195 binding, signifying the presence of activated microglia, persisted many months (>12) after antiviral treatment. Cortical areas that showed early high [^{11}C](*R*)-PK11195 binding subsequently underwent atrophy. These observations demonstrate that *in vivo* imaging of activated microglia/brain macrophages provides a dynamic measure of active tissue changes following an acute focal lesion. Importantly, the glial tissue response in the wake of neuronal damage is protracted and widespread within the confines of the affected distributed neural system and can be related to the long-term functional deficits.

Keywords: microglia; neuropsychology; inflammation; cognition

Abbreviations: BP = binding potential; HSV = herpes simplex virus; PBBS = peripheral benzodiazepine binding site; TAC = time-activity curves

Introduction

Post-mortem studies of patients after acute sporadic encephalitis caused by herpes simplex virus (HSV type 1) have shown that histological changes frequently occur far beyond the structurally defined primary lesion site (Esiri *et al.*, 1995; Esiri and Kennedy, 1997). Notably widespread is the presence of activated microglia (Weinstein *et al.*, 1990; Esiri *et al.*, 1995; Lellouch-Tubiana *et al.*, 2000), a cell type of mononuclear phagocyte lineage that represents an important part of the intrinsic immune defence of the CNS (Banati *et al.*, 1993; Kreutzberg, 1996). Two

mechanisms have been suggested to explain the distribution pattern of brain damage after herpes simplex encephalitis: (i) the inflammatory process progresses locally by spreading into areas of closest anatomical proximity; and (ii) the progressive tissue damage follows a 'connectionist' disease model; i.e. pathology outside the primary inflammatory focus is induced in distant areas via the degeneration of neural pathways to those areas (Hierons *et al.*, 1978; Kapur *et al.*, 1994).

PK11195 [1-(2-chlorophenyl)-*N*-methyl-*N*-(1-methylpropyl)-3-isoquinoline carboxamide] is a specific ligand for the peripheral benzodiazepine binding site (PBBS), which is particularly abundant on cells of mononuclear phagocyte lineage (Benavides *et al.*, 1988; Dubois *et al.*, 1988; Myers *et al.*, 1991; Gavish *et al.*, 1999). In normal brain tissue, binding of PK11195 is minimal, whereas in areas containing activated microglia, *in vivo* binding is significantly increased (Banati *et al.*, 1997; Conway *et al.*, 1998). [^{11}C]PK11195 or its single enantiomer, [^{11}C](*R*)-PK11195, and PET have been used to image focal accumulation of macrophages or activated microglia in patients with stroke or epilepsy (Ramsay *et al.*, 1992; Banati *et al.*, 1999; Pappata *et al.*, 2000). Astrocytes that express the binding sites for PK11195 *in vitro* (Itzhak *et al.*, 1993) do not contribute significantly to the binding of (*R*)-PK11195 *in vivo*, as shown by double immunocytochemical and high-resolution autoradiographic labelling at the single-cell level (Banati *et al.*, 2000). Likewise, astrocytic scars do not have an appreciable [^{11}C](*R*)-PK11195 signal in patients with hippocampal sclerosis and well-controlled seizures (Banati *et al.*, 1999).

In this study, we employed [^{11}C](*R*)-PK11195-PET and volumetric serial MRI to test whether the visualization of activated microglia/brain macrophages in the presence or absence of obvious structural changes provides a measure not only of the severity of a primary brain lesion but also of its secondary effects in antero- and retrograde neuronal projection pathways.

We specifically selected patients in whom the acute disease was largely confined to one temporal lobe to study (i) the distribution of the damage after herpes encephalitis including areas remote from the primary lesion site; (ii) the relationship between the presence of brain macrophage/activated microglia and regional brain atrophy over a longer period of time; and (iii) the relationship of these *in vivo* imaging data with the patients' specific cognitive deficits.

Material and methods

Subjects

Patients

Patient 1, a 44-year-old right-handed woman, was scanned with MRI and [^{11}C](*R*)-PK11195-PET 5 months after the acute onset of predominantly left-sided herpes simplex encephalitis. MRI and PET scans were repeated 12 months later, i.e. 17 months after onset of the disease. Neuropsychological assessment at the time of the first scans demonstrated severe deficits in verbal but not visual memory. The verbal memory index on the Wechsler Memory Scale—Revised was reduced to 71, compared with a visual memory index of 114. In the Recognition Memory Test, the patient's scores reached the 5th percentile for word recognition, compared with the 95th percentile for the face recognition memory test. Performance was within normal range on Raven's Progressive Matrices, the Graded Naming Test, and tests assessing frontal and executive functioning (Wisconsin Card-Sorting Test and FAS verbal fluency test). Whereas attention and concentration were normal, the Wechsler Memory Scale—Revised test showed a significant impairment in delayed recall. The patient's cognitive functions remained stable over the 12-month period of observation except for a slight deterioration in verbal memory.

Patient 2, a 36-year-old right-handed man, was scanned with MRI and [^{11}C](*R*)-PK11195-PET 8 months after the acute onset of herpes simplex encephalitis that affected predominantly the right temporal lobe. MRI and PET scans were repeated 6 months later, i.e. 14 months after disease onset.

At the time of the first scans, the patient showed a number of cognitive deficits, most prominently affecting visual memory and face processing. Deficits were seen on tests of spatial and visual recognition memory, and visual discrimination and reversal learning from the CANTAB (Cambridge Neuropsychological Test Automated Battery) (Cenes, Cambridge, UK). The deficit in visual memory appeared to be genuinely mnemonic in nature, as deficits increased with increasing delay on a test of delayed matching to sample from the CANTAB. Deficits in unfamiliar face matching (Benton Face Recognition Test), as well as deficits in facial emotion recognition (particularly for negative emotions, including fear, anger and disgust) were seen (Benton *et al.*, 1983; Broks *et al.*, 1998). There appeared to be relative sparing of performance on tests of aspects of social knowledge (Ellis *et al.*, 1994). No obvious change in the degree and pattern of cognitive deficits was seen over the period of observation.

The clinical diagnosis of herpes simplex encephalitis was confirmed in both patients by high titres of antibodies against HSV-1 and the detection of HSV-1 DNA in the cerebrospinal fluid using the polymerase chain reaction. Both patients were committed to an intensive care unit within 1 day after the onset of the acute illness. Patient 1 received 650 mg/day intravenous acyclovir for the 16 days, followed by a 4-week course of 1 g/day oral valacyclovir. Patient 2 was treated with 750 mg/day intravenous acyclovir for 14 days.

Control subjects

To determine binding potential values of [^{11}C](*R*)-PK11195 in the normal cortex and subcortical cerebral grey matter, a group of 13 healthy subjects (six women, seven men, age

range 33–80 years, mean age 53.2 years) were scanned for comparison.

The protocol for patients with inflammatory brain disease and controls was approved by the Royal Postgraduate Medical School, Hammersmith, Queen Charlotte's and Chelsea and Acton Hospitals Research Ethics Committee and the ARSAC (Administration of Radioactive Substances Advisory Committee of the UK). Written consent was obtained from all studied subjects and their carers.

PET study

Data acquisition

A CTI/Siemens (Knoxville, Tenn., USA) ECAT 953B PET scanner was used in 3D acquisition mode with collimating septa withdrawn. This produces a fivefold increase in counts at the centre of the field-of-view compared with that achieved using conventional scanning (Bailey *et al.*, 1991). In this study, the single enantiomer [^{11}C](*R*)-PK11195, which has a higher affinity for the PBBS than the racemic form, was used (Shah *et al.*, 1994). The ligand was injected as a bolus 30 s after the beginning of the acquisition scan. The tracer dose (mean ± standard deviation) was 360 ± 30 MBq with a specific activity of 37 ± 1 GBq/mmol. Dynamic data were collected over 60 min as 18 temporal frames. Attenuation correction factors were determined using a 15-min transmission scan. Scatter correction was achieved using a dual-energy window method (Groontoonk *et al.*, 1996). Data were reconstructed with a ramp filter at Nyquist cut-off producing a reconstructed image resolution of 5.8 mm (full-width at half-maximum) at the centre of the field of view.

Kinetic modelling and analysis

Parametric images of regional [^{11}C](*R*)-PK11195 binding were generated using a simplified reference tissue model (Lammertsma and Hume, 1996; Gunn *et al.*, 1997; Banati *et al.*, 1999, 2000; Cagnin *et al.*, 2001). In severe brain disease with widespread distribution of pathology throughout the entire brain, the *a priori* assumption that a given anatomically defined reference region is free of specific binding may not hold. Therefore, we used cluster analysis to classify tissues for the discrimination of concentration time–activity curves (TACs) according to their shape, in order to extract a normal ligand kinetic to serve as an appropriate reference input function (Ashburner *et al.*, 1996; Acton *et al.*, 1997; Gunn *et al.*, 1998; Myers *et al.*, 1999; Banati *et al.*, 2000). A normalized mean TAC (normal population input kinetic) derived from the healthy cortical brain tissue of a group of 13 control subjects was created, representing the shape of a TAC derived from regional tissue data with no or minimal binding. To ensure that a TAC extracted by cluster analysis (after segmentation into 10 clusters) from the raw dynamic data of a patient was appropriate to serve as the patient's reference ligand kinetic, i.e. a kinetic with the shape of a TAC from normal brain tissue, its shape was assessed by testing for dissimilarity with the previously established normal population input kinetic (χ^2-test, $P < 0.05$) (Fig. 1A and B). For validation, the parametric images obtained using cluster analysis were compared with those using a cerebellar reference region, as described previously (Banati *et al.*, 1999).

To allow anatomical localization of the regional [^{11}C](*R*)-PK11195 binding, the binding potential (BP) images were co-registered to and overlaid on the individuals' own MRIs (Studholme *et al.*, 1997). For the calculation of regional mean BP values, volumes of interest within the limbic system and anatomically connected areas were defined on the individuals' volumetric MRIs and applied to their parametric BP images using Analyze AVW version 3 (Robb and Hanson, 1991).

Additionally, the regional [^{11}C](*R*)-PK11195 lesion load, i.e. the relative volume (%) with increased signal within in a given region of increased mean BP, was calculated as described previously (Banati *et al.*, 1999).

MRI

Each subject underwent a 3D T_1-weighted MRI scan (voxel size 1 × 1 × 1.3 mm; 128 contiguous slices; repetition time 35 ms, echo time 6 ms; flip angle 35°) obtained with a 1.0 T Picker (Cleveland, OH, USA) HPQ MRI scanner for the purpose of co-registration with the PET image and, in control subjects, for the exclusion of incidental pathology (Studholme *et al.*, 1997). In both herpes encephalitis patients, the structural changes between the first and second MRI scans were assessed with a volumetric MRI technique that used a matching procedure based on summing the least-squares differences of pixel intensity values (Hajnal *et al.*, 1995). The changes between the first and second scans were displayed in a difference image produced by subtracting the first MRI image from the second.

Statistical analysis

Means, standard deviations and *Z* values were calculated to determine the significance of the regional increase in [^{11}C](*R*)-*PK11195* binding in each patient compared with the group of control subjects. *Z* values >1.6 (in the one-tailed *Z*-test, testing for increase in specific binding) were considered statistically significant ($P < 0.05$). Correlation analysis was performed using Pearson's correlation coefficient and regression analysis.

Results

Control subjects

Using cluster analysis for the extraction of the normal input kinetic, the BP for the cortex of healthy control subjects was

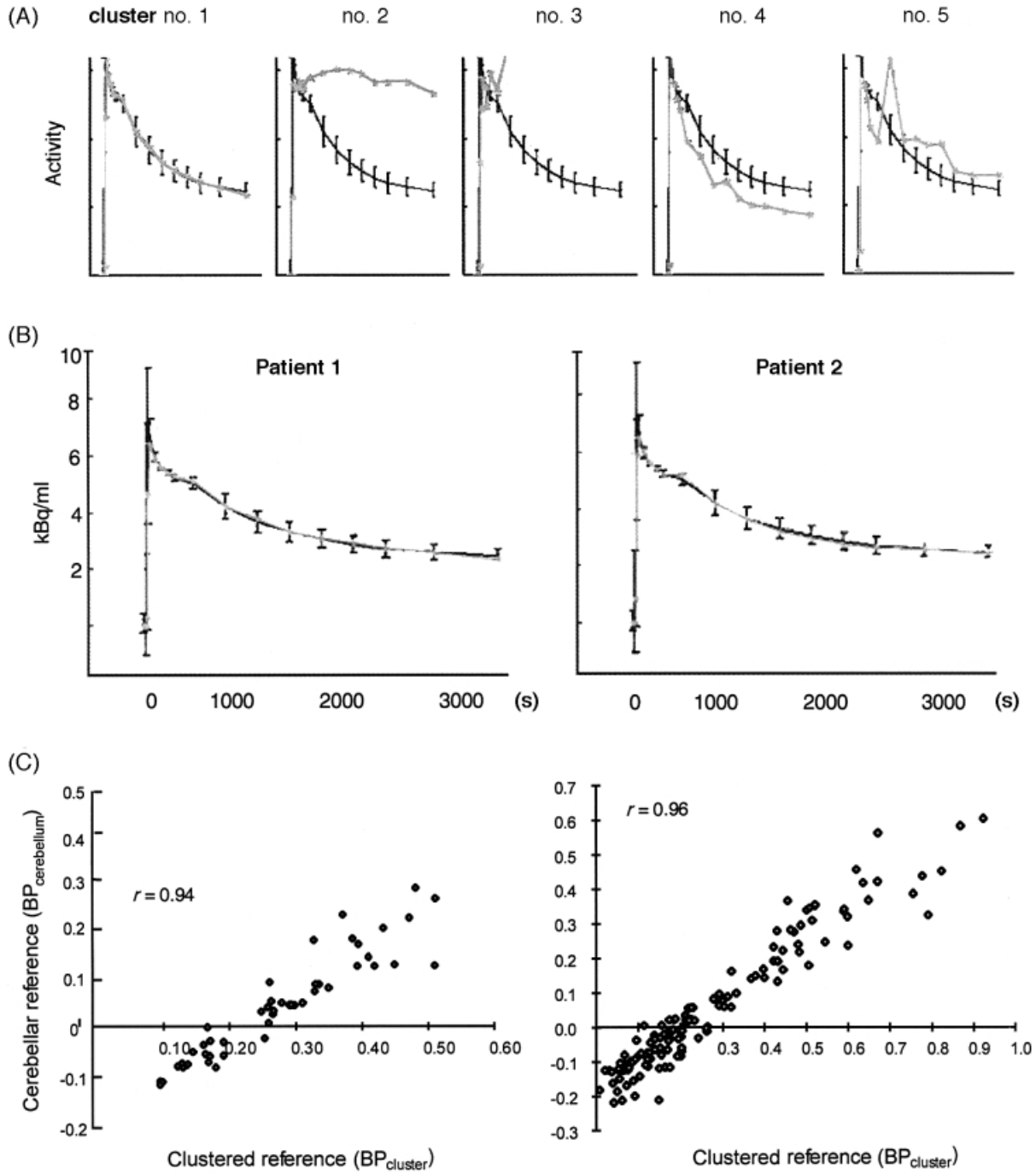

Fig. 1 Extraction of a normal ligand kinetic for reference input function. (**A**) The segmentation of dynamic raw data (here Patient 1) into 10 clusters (five of which are shown) of concentration time–activity curves (TACs; individual TACs are shown in light grey) discriminated by their shapes shows the presence of a TAC (cluster no. 1) similar to that found in normal cortex. (**B**) In both patients, a ligand kinetic with the shape of the TAC previously found to be characteristic of normal brain tissue (normal population input kinetic, shown as black curves; error bars denote standard deviations) were extracted and used as an appropriate reference input function (χ^2 test, $P < 0.001$ in both cases). (**C**) A good correlation of the regional binding potential (BP) values using cluster analysis for the extraction of a reference input kinetic with BP values using a cerebellar input function demonstrates that cluster analysis offers an alternative way of generating an input function for patients in whom the cerebellum itself is diseased and may, therefore, not be a suitable reference tissue. *Left*: $BP_{cerebellum}$ versus $BP_{cluster}$ in normal subjects; *Right*: $BP_{cerebellum}$ versus $BP_{cluster}$ in the herpes patients.

0.13 ± 0.04 (mean ± standard deviation) and that for the thalamus was 0.40 ± 0.08. These data indicate that, in the absence of any active pathology, [^{11}C](*R*)-PK11195 binding is minimal in the normal brain, except for some constitutive binding in the thalamus, which has been shown to increase with age (Cagnin *et al.*, 2001).

Table 1 *[^{11}C](R)-PK11195 binding potential (lesion load, %): Patient 1*

	Scan 1		Scan 2	
	Right	Left	Right	Left
Superior temporal gyrus	0.07	0.15	0.20* (13)	0.32*** (32)
Anterior	0.10	0.20* (10)	0.20* (14)	0.42*** (49)
Posterior	0.05	0.12	0.20* (13)	0.24** (19)
Inferior + middle temporal gyri	0.18	0.29*** (29)	0.16	0.44*** (50)
Anterior	0.20* (14)	0.40*** (44)	0.17	0.65*** (78)
Posterior	0.15	0.20* (15)	0.15	0.26*** (26)
Fusiform gyrus	0.17	0.49*** (53)	0.06	0.46*** (52)
Anterior	0.18	0.62*** (80)	0.09	0.79*** (86)
Posterior	0.16	0.47*** (50)	0.04	0.43*** (49)
Parahippocampal gyrus	0.23** (22)	0.92*** (97)	0.30*** (35)	0.59*** (66)
Hippocampal formation	0.22* (26)	0.82*** (91)	0.40*** (49)	0.67*** (78)
Amygdaloid complex	0.64*** (80)	0.78*** (91)	0.87*** (98)	0.76*** (87)
Insula	0.38*** (45)	0.43*** (52)	0.48*** (61)	0.43*** (58)
Orbitofrontal pole	0.32*** (32)	0.2* (14)	0.34*** (33)	0.28*** (29)
Anterior cingulate gyrus	0.5*** (64)	0.52*** (69)	0.31*** (33)	0.29*** (28)
Lingual gyrus	0.14	0.44*** (51)	0.09	0.59***
Inferior parietal lobule	0.13	0.12	0.15	0.19
Thalamus	0.48	0.60** (75)	0.51	0.60** (75)

*$P < 0.05$; **$P < 0.01$; ***$P < 0.001$.

Table 2 *[^{11}C](R)-PK11195 binding potential (lesion load, %): Patient 2*

	Scan 1		Scan 2	
	Right	Left	Right	Left
Superior temporal gyrus	0.17	0.06	0.09	0.12
Anterior	0.32*** (36)	0.05	0.13	0.17
Posterior	0.07	0.07	0.05	0.08
Inferior + middle temporal gyri	0.18	0.03	0.10	0.07
Anterior	0.23** (22)	0.06	0.20* (11)	0.12
Posterior	0.15	0.01	0.04	0.04
Fusiform gyrus	0.23** (22)	0.17	0.21* (27)	0.11
Anterior	0.26** (35)	0.26*** (29)	0.43*** (56)	0.10
Posterior	0.21* (12)	0.08	0.14	0.12
Parahippocampal gyrus	0.56*** (71)	0.21* (15)	0.37*** (47)	0.19
Hippocampal formation	–	0.14	–	0.15
Amygdaloid complex	–	0.43*** (57)	–	0.11
Insula	–	0.58*** (72)	–	0.33*** (32)
Orbitofrontal pole	0.42*** (47)	0.18	0.22** (47)	0.19
Anterior cingulate gyrus	0.51*** (65)	0.30*** (29)	0.23** (18)	0.22* (16)
Lingual gyrus	0.28*** (33)	0.06	0.13	0.09
Inferior parietal lobule	0.07	0.02	0.03	0.00
Thalamus	0.67*** (81)	0.46	0.55* (72)	0.51

*$P < 0.05$; **$P < 0.01$; ***$P < 0.001$.

Patients

In both patients, cluster analysis was used successfully (χ^2-test, $P < 0.001$) to extract a TAC that had the same shape as the normal population input kinetic described for normal brain tissue and could, therefore, be used as the reference input function for the calculation of BP. High specific binding of [^{11}C](*R*)-PK11195 was seen in well-delineated limbic structures and some anatomically connected areas, reaching maximal values (BP_{max} = 1.9–2.00) in focal areas, such as the primarily affected hippocampus. The regional mean BPs are summarized in Tables 1 and 2.

Patient 1

The T_1-weighted volumetric MRI at the time of the first PET scan showed a well-defined lesion with partial loss

of tissue in the left hippocampal formation (Fig. 2A–C). In contrast, the first [^{11}C](*R*)-PK11195-PET scan revealed a distributed pathology mostly within the limbic system, including the anterior parts of the left parahippocampal, fusiform, inferior and middle temporal gyri, the amygdaloid nuclei, the anterior cingulate gyrus, the orbitofrontal cortex and insulae bilaterally, the area of the anterior commissure and the fornices (Figs 2 and 3). Additionally, increased [^{11}C](*R*)-PK11195 binding was found in the thalamus ipsilateral to the primarily affected left temporal lobe. With the exception of the thalamus, structures with increased [^{11}C](*R*)-PK11195 binding in the first scan subsequently developed atrophic changes, as measured by MRI subtraction imaging 12 months later (Figs 2 and 3). The second [^{11}C](*R*)-PK11195-PET scan, 1 year later, revealed a wider distribution pattern of microglial activation. While there was still partial overlap with areas of previous binding in the hippocampal and parahippocampal formations, binding of [^{11}C](*R*)-PK11195 increased throughout the left temporal lobe, the right mesial temporal lobe with right insula, and both mammillary bodies (Fig. 2E). In areas that had developed severe atrophy (the hippocampal and parahippocampal formations and the anterior cingulate gyrus), the regional mean BP values remained significantly increased though slightly reduced, probably as a consequence of the loss of volume in these structures (Fig. 5).

Patient 2

MRI at the time of the first PET scan showed loss of tissue in the right hippocampal and parahippocampal formations, amygdala and insula and a decrease in signal intensity in the entire right temporal lobe. As in Patient 1, the neuroinflammatory pathology was distributed throughout the entire limbic system (Fig. 4). Binding of [^{11}C](*R*)-PK11195 detected by the first PET scan was seen diffusely in the right temporal lobe extending into the remaining area of the insular cortex, bilaterally in the orbitofrontal cortex and anterior cingulate gyri, in the contralateral left insula and the left amygdaloid nucleus. Coronal sections revealed increased signal in the white matter above the right circular sulcus of the insula, an area that contains the superior longitudinal fascicle. Importantly, increased [^{11}C](*R*)-PK11195 binding was present in circumscribed areas in the right inferior parietal lobe and the right lingual gyrus, destruction of which has been hypothesized to underlie deficits in the recognition of emotions in facial expressions (Adolphs *et al.*, 1996), such as those seen in this patient. The left hippocampal formation and temporal lobe were relatively spared, which is consistent with the preservation of verbal skills. Again, areas where the first PET scan indicated the presence of activated microglia/brain macrophages were found subsequently to undergo marked atrophy, as detected by subtraction MRI. In the second [^{11}C](*R*)-PK11195-PET scan, the anatomical pattern of active pathology, i.e. significantly increased binding, was largely maintained. BP values, however, were slightly reduced in all areas of pathology except the right anterior fusiform gyrus (Fig. 5).

Comparison of cluster analysis versus cerebellar reference region

The respective BP values for normal cortex and thalamus using a cerebellar input function were slightly lower [cortex, 0.0 $\pm$ 0.08 (mean $\pm$ standard deviation); thalamus, 0.15 $\pm$ 0.06] than those using the input function derived from cluster analysis. However, a good linear correlation was found between the BP values using a cluster analysis-derived input function and the BP values using a cerebellar input function [control group (BP values from thalamus, temporal lobe and pons): Pearson coefficient $r = 0.94$, $P > 0.01$; herpes patients: $r = 0.96$, $P > 0.01$) (Fig. 1C).

Discussion

Connecting anatomical pathways are the biological basis of models that describe the consequences of brain damage in terms of connectionist networks and ascribe the variations in the functional outcome to the varying extent to which different neural networks have been affected. This approach crucially requires the accurate delineation of the sustained focal damage and a measure of its effects on the wider anatomical connections applicable to the study of individual patients. In the two paradigmatic cases of (asymmetrical) herpes simplex encephalitis investigated here and followed over >1 year, [^{11}C](*R*)-PK11195-PET provided the important additional information that (i) after a focal brain lesion, activated microglia/brain macrophages can be found widely distributed and remote from sites of obvious structural damage, and that the [^{11}C](*R*)-PK11195-PET signal follows the location of the affected neural circuitry (in our cases, particularly the limbic structures and their connections); (ii) persistent microglial activation can be detected many months after successful antiviral treatment and cortical areas of high [^{11}C](*R*)-PK11195 binding may subsequently undergo atrophic structural changes; and (iii) the pattern of cognitive deficits in our patients reflected the lesion pattern, as delineated by the first [^{11}C](*R*)-PK11195-PET scan after recovery from acute illness.

Neuroinflammation, a non-neuronal surrogate marker of neuronal damage

The use of [^{11}C](*R*)-PK11195-PET to study the subacute and chronic evolution of brain injury introduces the concept of 'neuroinflammation'. It is based on the experimental observation that neuronal injury *per se*, in the absence of any other contributing pathology, such as damage to blood vessels, evokes a rapid, highly localized activation of microglia, the brain's intrinsic macrophages, around the

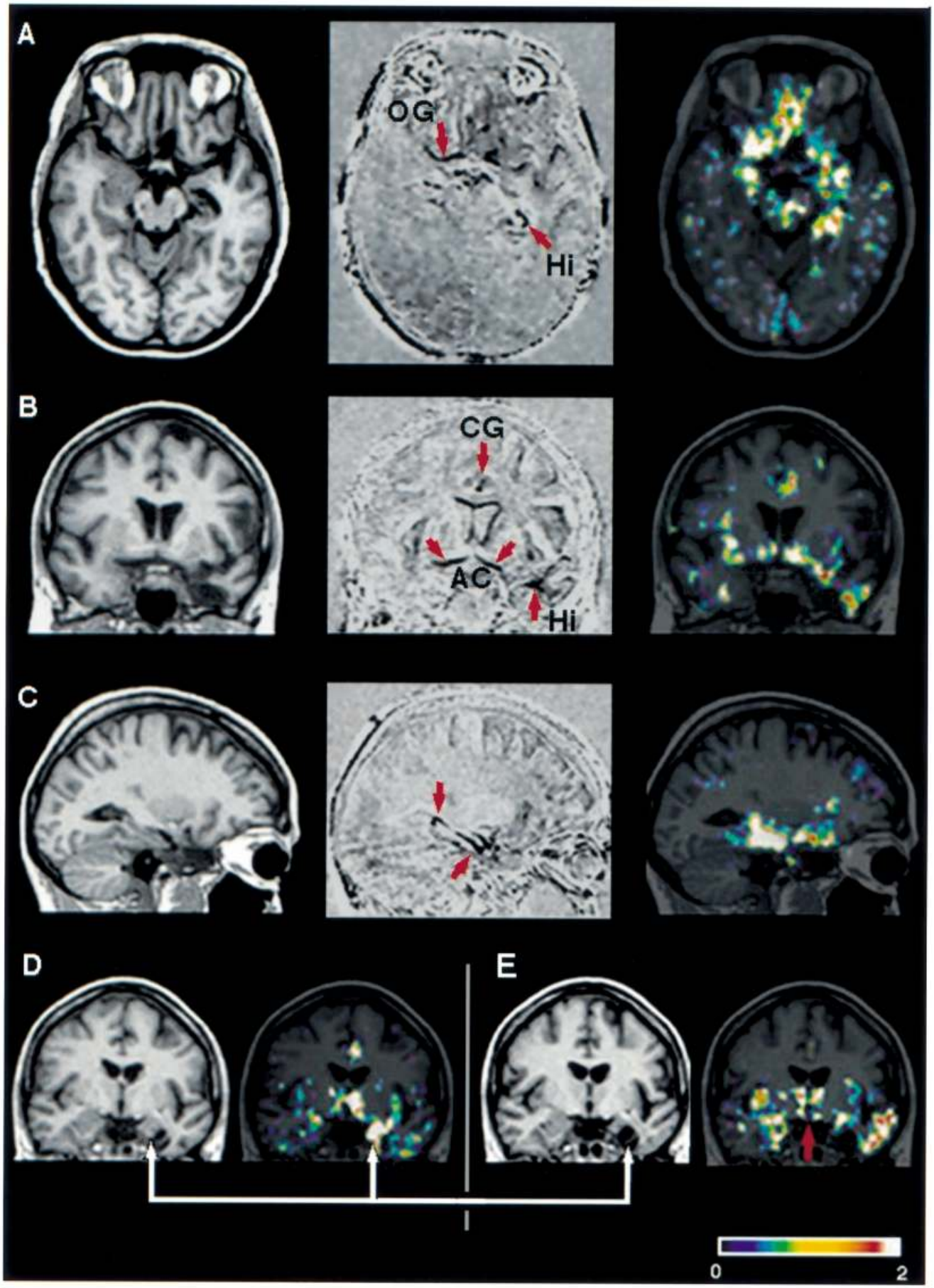
A
OG
Hi
B
CG
AC
Hi
C
D
E
0
2

somata of the injured neurones and in anatomical projection areas (Kreutzberg, 1996), which show no further obvious signs of pathology. This phenomenon is likely to have important functional consequences. For example, after nerve cell injury, even without cell death, discrete ultrastructural changes are observed, such as 'synaptic stripping', i.e. the protrusion of activated microglia into the synaptic clefts of the afferent synapses on the injured neurone (Blinzinger and Kreutzberg, 1968). It is conceivable that such subtle structural changes are one cellular correlate of functional disconnection in the absence of readily detectable anatomical abnormalities.

Peripheral nerve transection experiments demonstrate that neuroinflammatory responses are regularly projected bidirectionally along neural fibre tracts. For example, facial nerve transection leads to a retrograde neuronal reaction and rapid induction of microglial PK11195 binding sites around the somata of lesioned motor neurones in the facial nucleus, whereas after sciatic nerve transection an anterograde response with similar time-course occurs in the gracile nucleus in the brainstem, a projection area that contains synaptic terminals from long, ipsilaterally ascending nerve fibres (Kreutzberg, 1996; Banati *et al.*, 1997). In the case of herpes simplex encephalitis, the projecting axonal pathways along which microglial activation can occur consist of the large association bundles interconnecting the mesocortical areas, subicular allocortices and subcortical amygdaloid nuclei, which represent the anatomical circuit of Papez and together form the phylogenetically distinct unit of the limbic system (Damasio and Van Hoesen, 1985). In our patients, the distribution pattern of increased [^{11}C](*R*)-PK11195 binding delineated these limbic and associated structures and predicted the subsequent anatomical pattern of atrophy, as shown by MR difference imaging (Fig. 3).

The distribution of damage detected by the first [^{11}C](*R*)-PK11195-PET scan after recovery from acute illness was consistent with the pattern of the patients' cognitive deficits. For example, in Patient 2, who had predominantly right-sided herpes simplex encephalitis, [^{11}C](*R*)-PK11195-PET revealed a circumscribed, discrete pathology in the structurally normal right inferior parietal lobe [Brodmann area 39] and right lingual gyrus (mesial part, Brodmann area 18–19). Structural lesion analysis has indicated that these two regions are of critical importance in the recognition and processing of facial emotions, a cognitive function in which Patient 2 (in contrast to Patient 1) was markedly impaired (Adolphs *et al.*, 1996; Hamann *et al.*, 1996). Both regions are connected to the frontal lobes by the superior longitudinal fasciculus, a fibre tract that passes through the circular sulcus of the insula. In Patient 2, the superior longitudinal fasciculus co-localized on consecutive coronal planes with a contiguous signal of increased [^{11}C](*R*)-PK11195 binding (red circle in Fig. 4A). The increase in [^{11}C](*R*)-PK11195 binding in the morphologically normal right inferior parietal lobe and lingual gyrus of Patient 2 is likely to reflect a 'projected neuroinflammatory' response, i.e. the remote activation of microglia as a consequence of the severe damage to the frontotemporal gyri and the connecting superior longitudinal fasciculus, which also appears to be functionally relevant.

The findings of this study demonstrate that the pattern of microglial activation, as a surrogate marker of neuronal damage, helps to delineate the extent to which a focal lesion affects the distributed neural connectivities, which is not obvious when standard structural imaging techniques are used. Principally applicable to other forms of apparently focal brain damage, the study of glial responses should, therefore, help our understanding of the differences, so far unexplained, in the cognitive deficits in patients with apparently similar brain lesions (Eslinger *et al.*, 1993). The distribution pattern of activated microglia should also be of use for the precise histopathological description of the effects of neurotoxic lesions compared with focal structural

Fig. 2 Patient 1, with predominantly left-sided herpes encephalitis. This patient was scanned 5 and 17 months after onset of the disease. *Left*: T_1-weighted volumetric MRI 5 months after onset of disease. *Middle*: MRI subtraction image obtained by subtracting the patient's first MRI from a second MRI performed 12 months later. Areas of decreased signal intensity, e.g. due to loss of tissue, have become visible as dark structures. *Right*: [^{11}C](*R*)-PK11195 binding potential map of the first PET scan spatially transformed into MRI space and overlaid on the first MRI. Signals outside the brain, e.g. in the scalp, are masked. The colour bar denotes binding potential values between 0 and 2. (**A**) Transverse views showing pronounced signal loss due to atrophy (arrows in the MRI subtraction image) in the region of the right orbitofrontal gyrus (OG) and the left hippocampal formation (Hi). These areas of volume change had shown high binding in the [^{11}C](*R*)-PK11195-PET scan performed at the same time as the first MRI, indicating the presence of activated microglia/brain macrophages. (**B**) Coronal sections demonstrating damage to the left mesial temporal lobe in the first T_1-weighted MRI and atrophy (arrows) in the anterior cingulate (CG), left temporal lobe, orbitofrontal gyri and an area in the basal forebrain containing the substantia innominata and the anterior commissure (AC) in the MRI subtraction image (*middle*). There is also indication of atrophy of both insular cortices. Ventricular enlargement secondary to cortical pathology is demonstrated by a rim of signal change outlining the left lateral ventricle in the MRI subtraction image. The areas of MRI abnormalities are those of previous high [^{11}C](*R*)-PK11195 binding. (**C**) Sagittal sections showing the damage to the hippocampal formation and the increased [^{11}C](*R*)-PK11195 binding in the areas of MRI abnormalities and subsequent atrophy (arrows). (**D**) The first [^{11}C](*R*)-PK11195-PET scan revealed a high level of binding, mostly in the left mesial temporal lobe and the ipsilateral thalamus and (**E**) in contrast, the second MRI and PET scans (12 months after the first scans) show the disappearance of the hippocampal [^{11}C](*R*)-PK11195 binding due to necrosis (white arrows). The distribution of activated microglia/brain macrophages has now spread further into the left inferior, middle and superior temporal gyri and the contralateral right insular cortex, right mesial temporal structures and both mammillary bodies (red arrow).

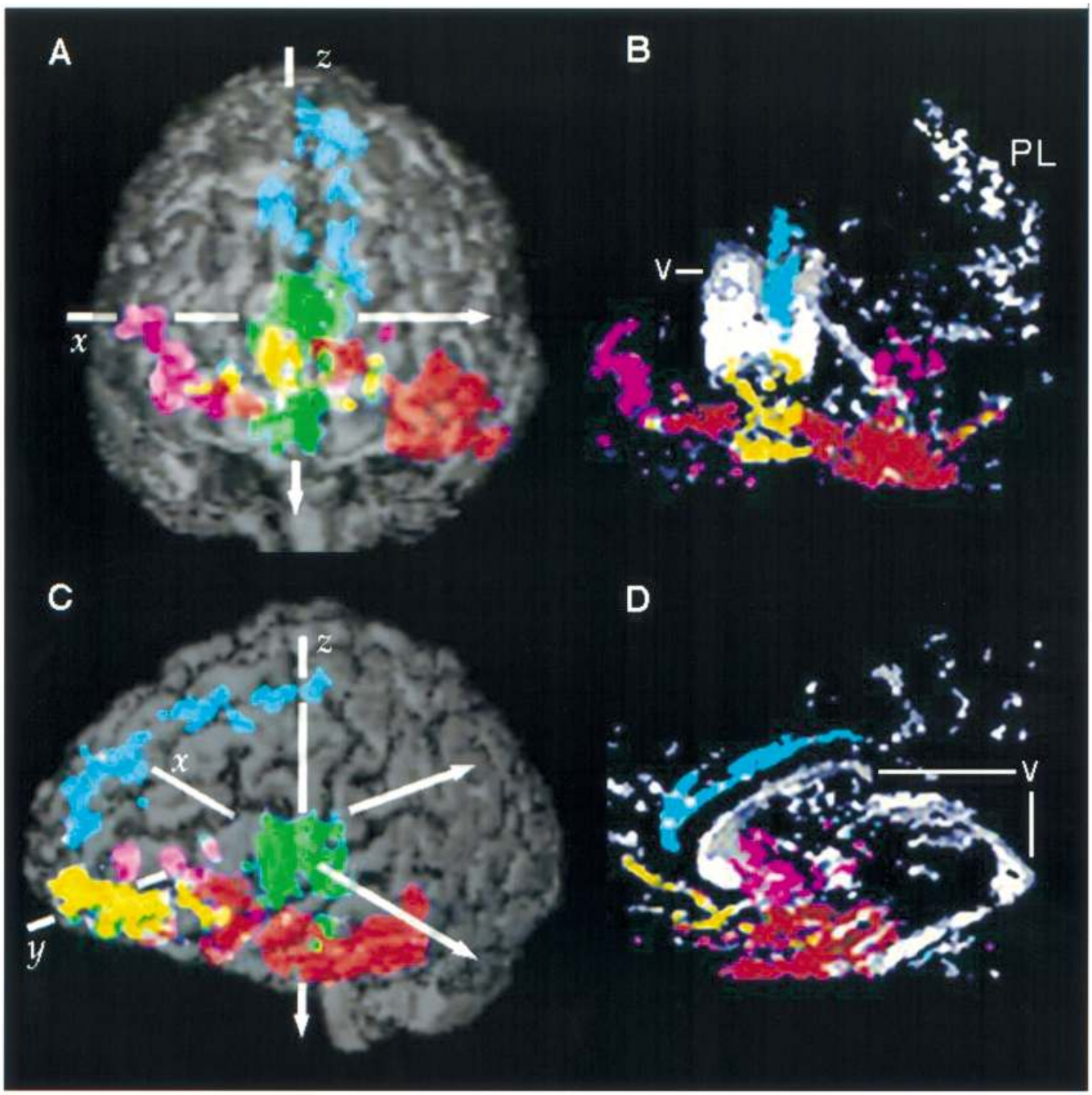

Fig. 3 Spatial relationship of activated microglia/brain macrophages with areas of subsequent atrophy (Patient 1). (**A** and **C**) The 3D [^{11}C](*R*)-PK11195 binding potential (BP) map (as a volume-rendered, binary image including all voxels with BP $>$ 2.5 $\times$ STD of background) projected onto the patient's MRI. (**B** and **D**) The volume-rendered MRI subtraction image (without extracerebral structures). The anatomical correlates of the areas of binding and atrophic changes are indicated by colours: blue = anterior cingulate; red = temporal lobe with hippocampal formation; green = thalamus and brainstem; purple = insular cortex; yellow = orbitofrontal gyri. Note that the [^{11}C](*R*)-PK11195 signal in the thalamus and brainstem is not associated with any volume changes in the MRI subtraction image. MRI subtraction images also show areas of change that reflect changes in brain mass rather than volume. Here, such a change, producing a low signal margin in the MRI subtraction image, can be seen in the left parietal lobe (PL), which is not normally involved in the disease and, as shown by [^{11}C](*R*)-PK11195-PET, was free of any active disease. Likewise, the loss of signal intensity around the ventricles (v) indicates in part a change and in part a secondary ventricular enlargement due to the distributed atrophy elsewhere.

lesions with respect to the observed variations in the functional outcome. Recent comparative studies of the functional deficits caused by the different types of experimental lesions to the hippocampus or adjacent regions have revealed damage that has been unaccounted for so far, and this has led to a reappraisal of the role of the

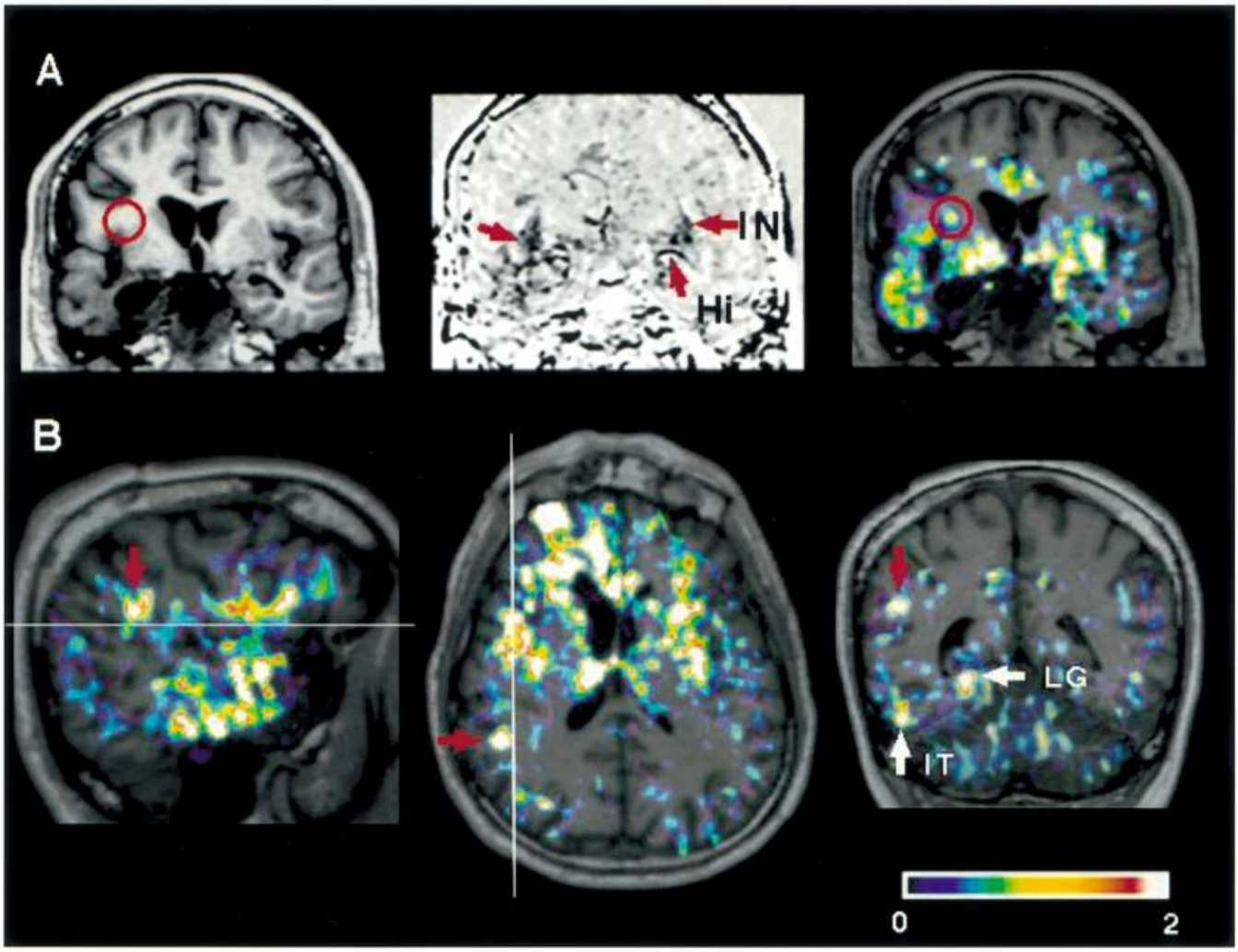

Fig. 4 Patient 2, who had predominantly right-sided herpes simplex encephalitis with involvement of the right inferior parietal lobe and lingual gyrus. This patient was scanned 8 months after the onset of disease and scanned again 6 months later. As in Patient 1, the areas of imminent or evolving atrophy (red arrows in the subtraction MRI (**A**, *middle*) are those characterized by high uptake of [^{11}C](*R*)-PK11195 in the first scan [**A**, *right*, [^{11}C](*R*)-PK11195 binding potential map overlaid on the first MRI (**A**, *left*)], particularly in the right temporal lobe, spreading through the ipsilateral (partially lost) insular cortex and inferior frontal gyrus, both anterior cingulate gyri, amygdaloid nuclei and left insula (IN). The red circle marks an area near the circular sulcus of the insula, through which passes the superior longitudinal fasciculus, which contains fibre tracts to the inferior parietal lobe and lingual gyrus. Hi = hippocampal formation. (**B**) Binding potential map of the first PET scan, shown spatially coregistered and overlaid on the first MRI scan, which shows an extended signal in the frontotemporal lobes and insula and an additional circumscribed area of high [^{11}C](*R*)-PK11195 uptake in the right inferior parietal lobe (red arrows) and right lingual gyrus (LG). IT = inferior temporal gyrus.

hippocampus in various aspects of memory (Goulet *et al.*, 1998; Murray *et al.*, 1998).

What is the significance of the persistent neuroinflammatory response?

The long persistence of elevated [^{11}C](*R*)-PK11195 signals and their further spread along the initially affected neural pathways many months after the onset of disease and clinical recovery is unlikely to have been due to continued viral activity. The assumption that the long-lasting inflammatory tissue response indicates continued activity of the virus itself is difficult to reconcile with the absence of any viral product after the first 3 weeks and the inconsistent detection of viral genome (Sobel *et al.*, 1989; Esiri *et al.*, 1995). While the detection of viral DNA may establish the latency of the virus in the central nervous system, the virus appears to be inactive and, therefore, the prolonged presence of post-infectious inflammatory changes must have a different cause. Recently, long-term persistent immune activation was found 3–10 years after acute childhood herpes simplex encephalitis, giving rise to the speculation that severe destructive brain infections

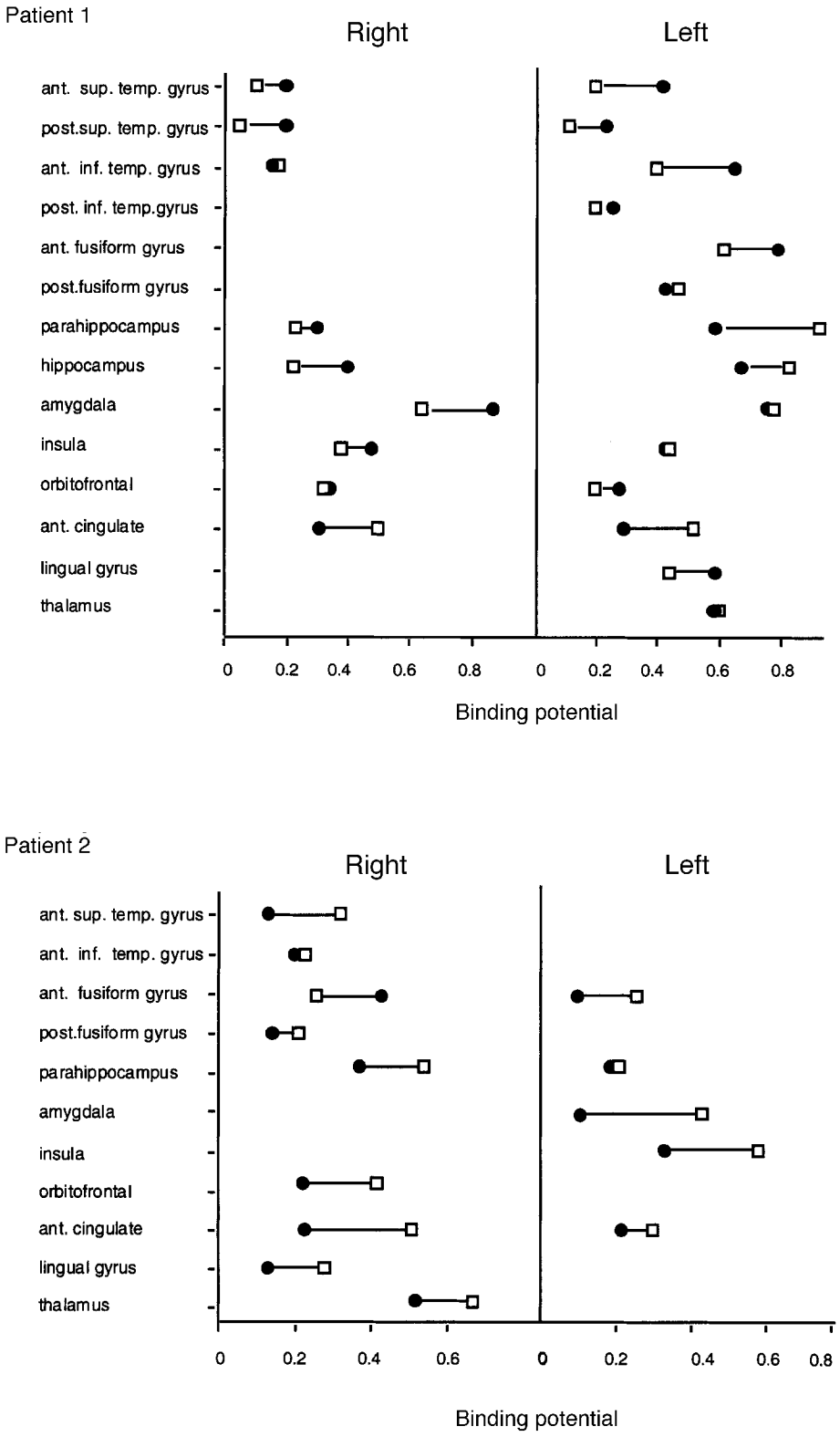

Fig. 5 Regional changes in [^{11}C](*R*)-PK11195 binding (open squares, first scan; closed circles, second scan). The profile of regional changes demonstrates a differential pattern of active pathology evolving over time. In Patient 1, the areas of highest binding in the first scan tend to show a reduction in binding, whereas neighbouring areas in the affected hemisphere and additional contralateral regions show an increase in binding. In Patient 2, who had a predominantly right-sided lesion, most regions, except the anterior part of the right fusiform gyrus, show a decrease in binding.

may cause self-induced immune activation similar to the secondary neuroinflammatory response seen in our study (Lellouch-Tubiana *et al.*, 2000). Similarly, even years after a single toxic event, such as in parkinsonism induced by MPTP (1-methyl-4-phenyl-1,2,3,6-tetrahydropyridine) (Langston *et al.*, 1999), activated microglia are present in selective areas, indicating a continuing or secondary neurodegenerative processes. A further important observation is that neuronal death alone, without blood–brain barrier damage, can lead to the recruitment of peripheral T lymphocytes and lead to the appearance of a classical inflammatory reaction despite the absence any infectious agent (Raivich *et al.*, 1998). Therefore, the presence of a persistent local immune reaction in the brain should not necessarily be equated with the presence of active infectious disease.

In the patients reported here, the presence of [^{11}C](*R*)-PK11195 signal after >1 year and in areas previously not delineated by the first [^{11}C](*R*)-PK11195-PET scan (Fig. 5), such as corresponding regions in the contralateral hemisphere (particularly in Patient 1) and other anatomically connected structures, such as the mammillary bodies, indicates not only the large scale but also the protracted time course of brain reorganization following focal damage. The delayed activation of microglia in additional areas appeared to be restricted to structures directly connected to the primary lesion site and was not accompanied by any obvious further deterioration in cognitive performance. This might suggest that the later additional [^{11}C](*R*)-PK11195 signals delineated primarily the Wallerian-type degeneration of axons and synaptic terminals of the neurones that were damaged initially. In this type of axonal degeneration, the majority of brain macrophages are derived from locally activated microglia, which initiate the phagocytosis of cellular debris (Lawson *et al.*, 1994).

Taken together, our data on a long-lasting, still evolving and neuronally induced glial response may indicate that, after brain damage, the connectionist model used to establish structure–function relationships should take into account a network architecture that is less static than is often assumed implicitly. It remains to be studied in greater detail whether this might have implications for the rehabilitation of patients with brain damage and whether it may be advantageous to reduce the secondary effect on initially undamaged neural systems that could potentially participate in the long-term rehabilitation of lost cognitive functions.

Methodological considerations

Our data show that, despite some small systematic differences in the calculated BP values depending on whether a cerebellar or a cluster analysis-derived input function was used, there was no difference in the overall anatomical pattern of significant binding. This suggests that the cerebellum, if it is indeed spared of significant disease, can serve as a reference tissue. Provided that either method is applied consistently in both patients and controls, the anatomical patterns of pathology that are obtained will not differ. More importantly, our results demonstrate that cluster analysis is a feasible approach to defining a reference input function in brain diseases that do not spare the cerebellum. As discussed previously (Banati *et al.*, 2000), the BP obtained using the simplified reference tissue (Gunn *et al.*, 1997) is an estimate of the true binding and may contain small errors due to minimal amounts of specific binding in normal white and grey matter.

In summary, the particular value of [^{11}C](*R*)-PK11195-PET lies in the ability of [^{11}C](*R*)-PK11195 to bind to brain macrophages/microglia as sensors of neuronal injury. In addition to structural neuroimaging, this technique thus provides a cell-biological measure of *active* disease, the resulting neuronal disconnection, and the protracted large-scale reorganization of the brain following damage to specific regions or pathways.

Acknowledgements

The volumetric MRI analysis was carried out at the MRI Steiner Unit (Professor G. M. Bydder), Imperial College School of Medicine, Hammersmith Hospital, London, UK. We appreciate the support of Professor M. Kopelman, St Thomas's Hospital, London, in the recruitment and assessment of Patient 1. We thank the radiographers A. Blyth, D. Griffith and J. Holmes and Dr P. Bloomfield and L. Schnorr for assistance in image reconstruction, Professor R. Y. Moore, Pittsburgh, and Dr S. Rajeswaran for critical reading of the manuscript and Professor D. J. Brooks for his support of the overall research programme. R.B.B. is funded by the Medical Research Council and received support from L. D. Wedmore, the Multiple Sclerosis Society of Great Britain and Northern Ireland, the Max Planck Institute of Neurobiology (Martinsried, Germany) and the Deutsche Forschungsgemeinschaft grant 'The mitochondrial benzodiazepine receptor as indicator of early CNS pathology, clinical application in PET'. A.C. is supported by a Fellowship from the European Community (BMH4/CT98/5100) in the Training and Mobility of Researchers Programme in Biomedicine.

References

Acton PD, Pilowsky LS, Costa DC, Ell PJ. Multivariate cluster analysis of dynamic iodine-123 iodobenzamide SPET dopamine D2 receptor images in schizophrenia. Eur J Nucl Med 1997; 24: 111–8.

Adolphs R, Damasio H, Tranel D, Damasio AR. Cortical systems for the recognition of emotion in facial expressions. J Neurosci 1996; 16: 7678–87.

Ashburner J, Haslam J, Taylor C, Cunningham VJ, Jones T. A cluster analysis approach for the characterization of dynamic PET data. In: Myers R, Cunningham V, Bailey D, Jones T, editors. Quantification of brain function using PET. San Diego: Academic Press; 1996. p. 301–6.

Bailey DL, Jones T, Spinks TJ, Gilardi MC, Townsend DW. Noise equivalent count measurements in a neuro-pet scanner with retractable septa. IEEE Trans Med Imag 1991; 10: 256–60.

Banati RB, Graeber MB. Surveillance, intervention and cytotoxicity: is there a protective role of microglia? [Review]. Dev Neurosci 1994; 16: 114–27.

Banati RB, Gehrmann J, Schubert P, Kreutzberg GW. Cytotoxicity of microglia. [Review]. Glia 1993; 7: 111–8.

Banati RB, Myers R, Kreutzberg GW. PK ('peripheral benzodiazepine')-binding sites in the CNS indicate early and discrete brain lesions: microautoradiographic detection of [3H] PK11195 binding to activated microglia. J Neurocytol 1997; 26: 77–82.

Banati RB, Goerres GW, Myers R, Gunn RN, Turkheimer FE, Kreutzberg GW, et al. [11C](*R*)-PK11195 positron emission tomography imaging of activated microglia in vivo in Rasmussen's encephalitis. Neurology 1999; 53: 2199–203.

Banati RB, Newcombe J, Gunn RN, Cagnin A, Turkheimer F, Heppner F, et al. The peripheral benzodiazepine binding site in the brain in multiple sclerosis: quantitative in vivo imaging of microglia as a measure of disease activity. Brain 2000; 123: 2321–37.

Benavides J, Cornu P, Dennis T, Dubois A, Hauw J-J, MacKenzie ET, et al. Imaging of human brain lesions with an omega 3 site radioligand. Ann Neurol 1988; 24: 708–12.

Benton AL, Hamsher KS, Varney N, Spreen O. Contributions to neuropsychological assessment: a clinical manual. New York: Oxford University Press; 1983.

Blinzinger K, Kreutzberg G. Displacement of synaptic terminals from regenerating motoneurons by microglial cells. Z Zellforsch Mikrosk Anat 1968; 85: 145–57.

Broks P, Young AW, Maratos EJ, Coffey PJ, Calder AJ, Isaac CL, et al. Face processing impairments after encephalitis: amygdala damage and recognition of fear. Neuropsychologia 1998; 36: 59–70.

Cagnin A, Myers R, Gunn RN, Turkheimer FE, Cunningham VJ, Brooks DJ, et al. Imaging activated microglia in the ageing human brain. In: Gjedde A, Hansen SB, Knudsen GM, Paulson OB, editors. Physiological imaging of the brain with PET. San Diego: Academic Press; 2001. p. 361–7.

Conway EL, Gundlach AL, Craven JA. Temporal changes in glial fibrillary acidic protein messenger RNA and [3H]PK11195 binding in relation to imidazoline-I2-receptor and alpha 2-adrenoceptor binding in the hippocampus following transient global forebrain ischaemia in the rat. Neuroscience 1998; 82: 805–17.

Damasio AR, Van Hoesen GW. The limbic system and the localisation of herpes simplex encephalitis. J Neurol Neurosurg Psychiatry 1985; 48: 297–301.

Dubois A, Benavides J, Peny B, Duverger D, Fage D, Gotti B, et al. Imaging of primary and remote ischaemic and excitotoxic brain lesions. An autoradiographic study of peripheral type benzodiazepine binding sites in the rat and cat. Brain Res 1988; 445: 77–90.

Ellis HD, Ellis DM, Fraser W, Deb S. A preliminary study of right hemisphere cognitive deficits and impaired social judgements among young people with Asperger syndrome. Eur Child Adolesc Psychiatry 1994; 3: 255–66.

Esiri MM, Kennedy PGE. Viral diseases. In: Graham DI, Lantos PL, editors. Greenfield's neuropathology, Vol. 2. 6th ed. London: Arnold; 1997. p. 3–63.

Esiri MM, Drummond CW, Morris CS. Macrophages and microglia in HSV-1 infected mouse brain. J Neuroimmunol 1995; 62: 201–5.

Eslinger PJ, Damasio H, Damasio AR, Butters N. Non-verbal amnesia and asymmetric cerebral lesions following encephalitis. Brain Cogn 1993; 21: 140–52.

Gavish M, Bachman I, Shoukrun R, Katz Y, Veenman L, Weisinger G, Weizman A. Enigma of the peripheral benzodiazepine receptor. [Review]. Pharmacol Rev 1999; 51: 629–50.

Goulet S, Dore FY, Murray EA. Aspiration lesions of the amygdala disrupt the rhinal corticothalamic projection system in rhesus monkeys. Exp Brain Res 1998; 119: 131–40.

Grootoonk S, Spinks TJ, Sashin D, Spyrou NM, Jones T. Correction for scatter in 3D brain PET using a dual energy window method. Phys Med Biol 1996; 41: 2757–74.

Gunn RN, Lammertsma AA, Hume SP, Cunningham VJ. Parametric imaging of ligand receptor binding in PET using a simplified reference region model. Neuroimage 1997; 6: 279–87.

Gunn RN, Lammertsma AA, Cunningham VJ. Parametric imaging of ligand-receptor interactions using a reference tissue model and cluster analysis. In: Carson RE, Daube-Witherspoon ME, Herscovitch P, editors. Quantitative functional brain imaging with positron emission tomography. San Diego: Academic Press; 1998. p. 401–6.

Hamann SB, Stefanacci L, Squire LR, Adolphs R, Tranel D, Damasio A. Recognizing facial emotion. Nature 1996; 379: 497.

Hierons R, Janota, I, Corsellis JA. The late effects of necrotizing encephalitis of the temporal lobes and limbic areas: a clinico-pathological study of 10 cases. Psychol Med 1978; 8: 21–42.

Itzhak Y, Baker L, Norenberg MD. Characterization of the peripheral-type benzodiazepine receptors in cultured astrocytes: evidence for multiplicity. Glia 1993; 9: 211–8.

Kapur N, Barker S, Burrows EH, Ellison D, Brice J, Illis LS, et al. Herpes simplex encephalitis: long term magnetic resonance imaging and neuropsychological profile. J Neurol Neurosurg Psychiatry 1994; 57: 1334–42.

Kreutzberg GW Microglia: a sensor for pathological events in the CNS. [Review]. Trends Neurosci 1996; 19: 312–8.

Lammertsma AA, Hume SP. Simplified reference tissue model for PET receptor studies. Neuroimage 1996; 4: 153–8.

Langston JW, Forno LS, Tetrud J, Reeves AG, Kaplan JA, Karluk D. Evidence of active nerve cell degeneration in the substantia nigra of humans years after 1-methyl-4-phenyl-1,2,3,6-tetrahydropyridine exposure. Ann Neurol 1999; 46: 598–605.

Lawson LJ, Frost L, Risbridger J, Fearn S, Perry VH. Quantification of the mononuclear phagocyte response to Wallerian degeneration of the optic nerve. J Neurocytol 1994; 23: 729–44.

Lellouch-Tubiana, Fohlen M, Robain O, Rozenberg F. Immunocytochemical characterization of long-term persistent immune activation in human brain after herpes simplex encephalitis. Neuropath Appl Neurobiol 2000; 26: 285–94.

Murray EA, Barker MG, Gaffan D. Monkeys with rhinal cortex damage or neurotoxic hippocampal lesions are impaired on spatial scene learning and object reversals. Behav Neurosci 1998; 112: 1291–303.

Myers R, Manjil LG, Cullen BM, Price GW, Frackowiak RS, Cremer JE. Macrophage and astrocyte populations in relation to [3H]PK11195 binding in rat cerebral cortex following a local ischaemic lesion. J Cereb Blood Flow Metab 1991; 11: 314–22.

Myers R, Gunn RN, Cunningham VJ, Banati RB, Jones T. Cluster analysis and the reference tissue model in the analysis of clinical [^{11}C]PK11195-PET. J Cereb Blood Flow Metab 1999; 19 Suppl: S789.

Pappata S, Levasseur M, Gunn RN, Myers R, Crouzel C, Syrota A, et al. Thalamic microglial activation in ischemic stroke detected in vivo by PET and [11C]PK11195. Neurology 2000; 55: 1052–4.

Raivich G, Jones LL, Kloss CU, Werner A, Neumann H, Kreutzberg GW. Immune surveillance in the injured nervous system: T-lymphocytes invade the axotomized mouse facial motor nucleus and aggregate around sites of neuronal degeneration. J Neurosci 1998; 18: 5804–16.

Ramsay SC, Weiller C, Myers R, Cremer JE, Luthra SK, Lammertsma AA, et al. Monitoring by PET of macrophage accumulation in brain after ischaemic stroke. Lancet 1992; 339: 1054–5.

Robb RA, Hanson DP. A software system for interactive and quantitative visualization of multidimensional biomedical images. Australas Phys Eng Sci Med 1991; 14: 9–30.

Shah F, Hume SP, Pike VW, Ashworth S, McDermott J. Synthesis of the enantiomers of [N-methyl-11C]PK11195 and comparison of their behaviours as radioligand for PK binding sites in rats. Nucl Med Biol 1994; 21: 573–81.

Snedecor GW, Cochran WG. Statistical methods. 7th edition. Ames (IA): Iowa State University Press; 1980.

Sobel RA, Collins AB, Colvin RB, Bhan AK. The in situ cellular immune response in acute herpes simplex encephalitis. Am J Pathol 1986; 125: 332–8.

Studholme C, Hill DL, Hawkes DJ. Automated three dimensional registration of magnetic resonance and positron emission tomography brain images by multiresolution optimization of voxel similarity measures. Med Phys 1997; 24: 25–35.

Weinstein DL, Walker DG, Akiyama H, McGeer PL. Herpes simplex virus type I infection of the CNS induces major histocompatibility complex antigen expression on rat microglia. J Neurosci Res 1990; 26: 55–65.

Received March 19, 2001. Revised May 28, 2001.
Accepted June 11, 2001